Relativistic calculations of photoemission spectra of CoAl(110)

Relativistic calculations of photoemission spectra of CoAl(110)

D Mayer†, B Willerding†, K Wandelt†, G R Castro‡ and J Braun§

† Institut für Physikalische und Theoretische Chemie, Universität Bonn, 53115 Bonn, Germany
‡ European Synchrotron Radiation Facility, BP 220, 38043 Grenoble, France
§ Universität Osnabrück, Fachbereich Physik, 49069 Osnabrück, Germany

Abstract. Photoemission spectra obtained from the (110) surface of the ordered CoAl alloy, calculated in the framework of a fully relativistic one-step model of photoemission, are presented. The comparison of the theoretical spectra with experimental results shows good agreement over a wide range of photon energies and emission angles. Additionally we simulate partial disorder by taking into consideration Co antistructure atoms.

1. Introduction

The one-step model of photoemission, originally formulated by Pendry [1], is a useful tool for the understanding of angle-resolved ultraviolet photoemission (ARUPS) spectra. Nowadays, the model includes relativistic effects [2–5], the possibility of having several atoms per unit cell [6] and a realistic model for the surface potential [7, 8]. In the framework of this model, photoemission spectra of the stoichiometric binary alloy CoAl(110) were calculated for several photon energies and different orientations of polarization and emission angles. The bulk potentials in use were calculated by Ufer [9] within the tight-binding LMTO method.

The calculated spectra are compared with experimental results obtained by one of the authors [10] using synchrotron radiation. The experiments were always set up with the polarization vector of the electromagnetic field lying in the scattering plane defined by the directions of incident light and detected electrons. The experiments were performed along the $\overline{\Gamma}\,\overline{X}$ and the $\overline{\Gamma}\,\overline{Y}$ directions. The experimental spectra shown in this contribution were normalized to equal photocurrent emitted from a gold foil since the intensity of the synchrotron radiation varies with photon energy and time.

The electronic structure of CoAl is of both technological and theoretical interest. Because of its high melting point and high stability, this alloy is especially attractive for high-temperature applications [11]. The good strength-to-weight ratio and the high corrosion and oxidation resistance extend the field of application [12].

CoAl persists over a wide composition range (46–58 at.% Co [13]). The main reasons for this variation from stoichiometry are Co antistructure atoms in the Al sublattice and vacancies in the Co sublattice [14]. Therefore we tried to simulate the random deviations from stoichiometric composition by using larger unit cells each with one Co antistructure atom.

It should be mentioned here that a wealth of experimental and theoretical results are available for NiAl, which also is a transition metal aluminide. Quantitative I–V LEED

and angle-resolved photoemission measurements for example can be found in the literature [15, 18, 19], as well as theoretical investigations concerning the electronic structure of this compound performed by using the LAPW method [17] and the full-potential LAPW method [19]. Furthermore, self-consistent electronic structure calculations, based on pseudo-potentials [18], as well as calculations of the oscillatory surface relaxation [16] have been carried out.

2. Theory

A detailed description of the relativistic photoemission theory is given elsewhere [20]. Therefore, we present here only the basic formulae of a relativistic one-step theory. In the framework of the one-step model of photoemission, the spin-averaged electron current is given by the following expression:

$$I(\mathbf{k}_\parallel, \epsilon_f) = -\frac{1}{\pi} \text{Im} \langle \mathbf{k}_\parallel, \epsilon_f | G_2^+ \Delta G_1^+ \Delta^+ G_2^- | \mathbf{k}_\parallel, \epsilon_f \rangle. \tag{1}$$

$G_2^\pm$ and G_1^+ are 4×4 matrices and denote the relativistic retarded (G^+) and advanced (G^-) single-particle Green functions for the final (G_2) and the initial state (G_1). In a relativistic theory, the interaction of an electron with the electromagnetic field is described by the operator

$$\Delta = -\boldsymbol{\alpha} \cdot \mathbf{A}_0 \tag{2}$$

where $\mathbf{A}_0$ denotes the spatially constant amplitude of the electromagnetic vector potential. The three components α_k of the vector $\boldsymbol{\alpha}$ are defined through the tensor product

$$\alpha_k = \sigma_1 \otimes \sigma_k \qquad k = 1, 2, 3$$

where the σ_k denote the Pauli spin matrices.

In the space representation we obtain

$$\rho = -\frac{1}{\pi} \text{Im} \int d\mathbf{r} \int d\mathbf{r}' \ \Psi_f^\dagger(\mathbf{r}) \Delta G_1^+(\mathbf{r}, \mathbf{r}') \Delta^\dagger \Psi_f(\mathbf{r}') \tag{3}$$

with the time-reversed SPLEED state

$$\Psi_f^\dagger(\mathbf{r}) = \langle \mathbf{r} | G_2^+ | \epsilon_f, \mathbf{k}_\parallel \rangle. \tag{4}$$

The spin-averaged photocurrent I follows:

$$I = \text{tr}(\rho). \tag{5}$$

As a consequence of multiple-scattering theory, the spin-density matrix is divided into four different contributions:

$$\rho(\epsilon_f, \mathbf{k}_\parallel) = \rho^{\text{atom}}(\epsilon_f, \mathbf{k}_\parallel) + \rho^{\text{intra}}(\epsilon_f, \mathbf{k}_\parallel) + \rho^{\text{inter}}(\epsilon_f, \mathbf{k}_\parallel) + \rho^{\text{surf}}(\epsilon_f, \mathbf{k}_\parallel). \tag{6}$$

Evaluation of the atomic contribution ρ^{atom} for a semi-infinite crystal gives

$$\rho^{\text{atom}}(\epsilon_f, \mathbf{k}_\parallel) = \frac{1}{\pi} \text{Im} \left(ik_1 \sum_{jn} \sum_{\kappa\kappa'\kappa''} \sum_{\mu\mu'\mu''} A_{j\kappa}^{\mu n} D_{\kappa\mu\kappa'\mu'} M_{\kappa\kappa'\kappa''}^n D_{\kappa'\mu'\kappa''\mu''}^* A_{j\kappa''}^{\mu''*n} \right). \tag{7}$$

Herein $A_{j\kappa}^{\mu n}$, $D_{\kappa\mu\kappa'\mu'}$ and $M_{\kappa\kappa'\kappa''}^n$ denote the spherical coefficients for the final-state wave field, the angular matrix elements and the radial double-matrix elements. The summation indices n and j denote the n'th atom in the unit cell and the j'th layer of the semi-infinite crystal.

Evaluation of the multiple-scattering contributions $\rho^{\text{intra,inter}}$, involving the multiple scattering of the initial state inside and between the bulk crystal layers, results in

$$\rho^{\text{intra+inter}}(\epsilon_f, \boldsymbol{k}_\parallel) = \frac{1}{\pi} \text{Im}\left(i k_1 \sum_{jn} \sum_{\kappa\kappa'} \sum_{\mu\mu'} A_{j\kappa}^{\mu n} \tilde{M}_{\kappa\kappa'}^n D_{\kappa\mu\kappa'\mu'} (B_{j\kappa'}^{\mu'n} + G_{j\kappa'}^{\mu'n}) \right). \tag{8}$$

Herein $B_{j\kappa'}^{\mu'n}$ and $G_{j\kappa'}^{\mu'n}$ denote the spherical coefficients for the intralayer (interlayer) part of the initial-state wave field and $\tilde{M}_{\kappa\kappa'}^n$ the radial single-matrix elements. Final evaluation of the surface contribution gives

$$\rho^{\text{surf}}(\boldsymbol{k}_\parallel, \epsilon_f) = -\frac{1}{\pi} \frac{A_z}{2\omega c} \text{Im}\left(e^{i\boldsymbol{q}_\parallel \cdot \boldsymbol{c}_{1\parallel}} \sum_{gs} \int_{-\infty}^{c_{1z}} dz \; \psi_{2gs}(z) \frac{dV_B}{dz} \phi_{1gs}(z) e^{iq_z z} \right). \tag{9}$$

Herein $\phi_{1gs}(z)$ and $\psi_{2gs}(z)$ denote the regular solutions of the Schrödinger equation to the spin index s for $V_B(z)$ in the range $-\infty < z < c_{1z}$. The value c_{1z} defines the point where the surface potential goes smoothly into the inner potential of the bulk crystal. A_z is the z-component of the amplitude $\boldsymbol{A}_0$ and $\boldsymbol{q}$ is the wave vector of the photon field.
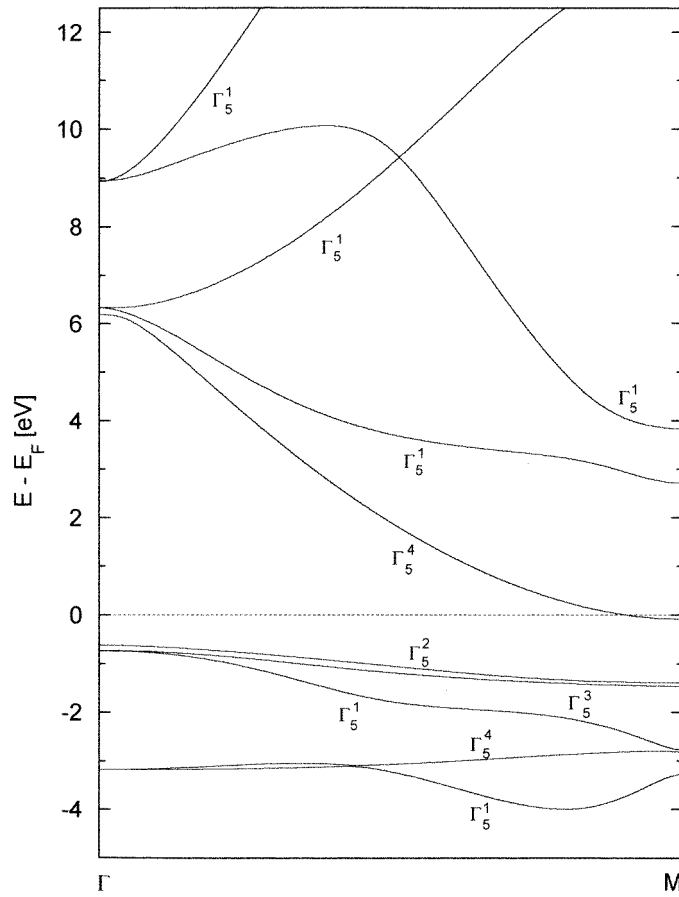

Figure 1. The KKR bandstructure of an infinite CoAl crystal.

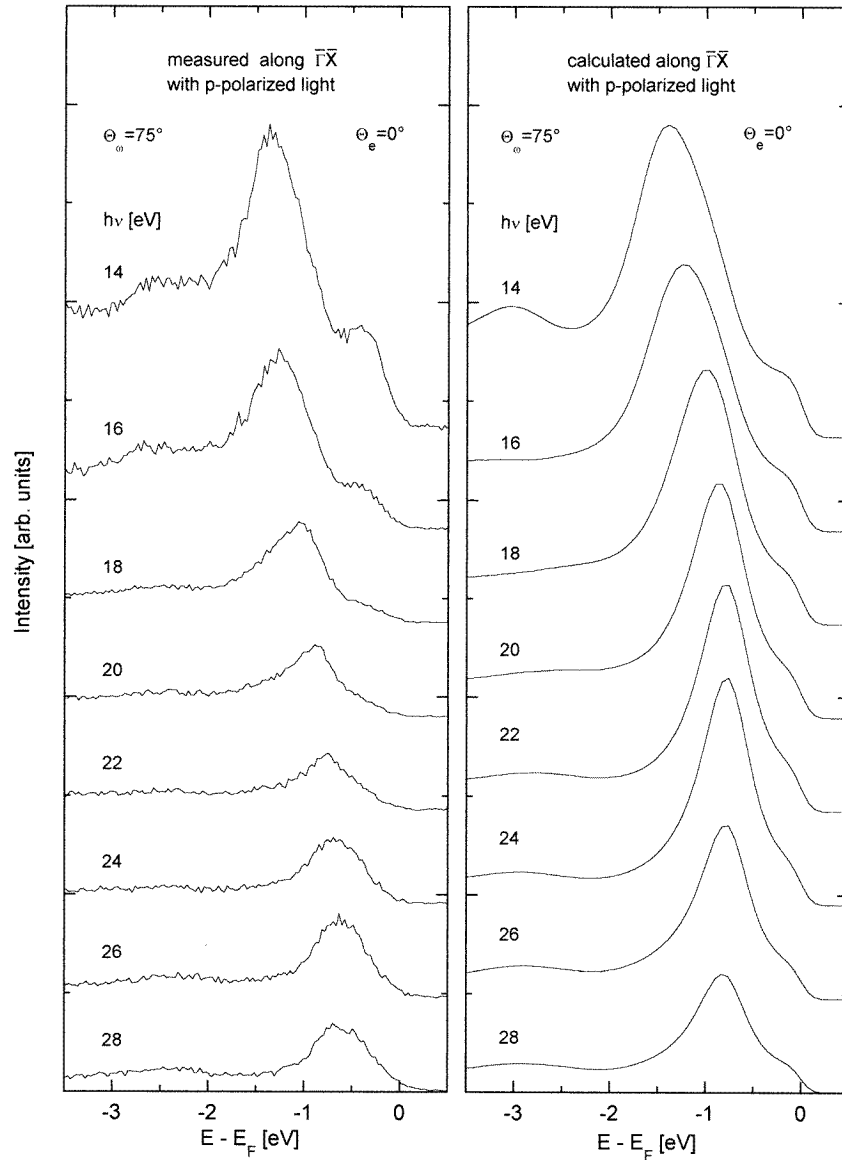**Figure 2.** A series of normal-emission spectra for different photon energies obtained using p-polarized light along $\overline{\Gamma}\,\overline{X}$. Left: experimental spectra; right: calculated spectra (angle of photon incidence $\Theta_\omega = 75°$; angle of electron emission $\Theta_e = 0°$).

3. Methods of calculation

In order to calculate the bulk potentials for CoAl in the CsCl structure we have applied the tight-binding linear muffin-tin orbital method [21, 22] in the atomic sphere approximation (TB-LMTO-ASA), by using equal and space-filling atomic sphere radii on Al and Co sites. According to previous studies [23], this choice, for example for CoAl, results in an optimal description of the electron density in the ASA. Exchange–correlation effects are considered

according to the exchange–correlation potential given by von Barth and Hedin [24]. For both constituent atoms, basis functions up to $l = 2$ were used explicitly, whereas $l = 3$ functions have been included via the downfolding procedure [25, 26]. Furthermore, the effect of non-local corrections [27, 28] to the local density approximation has been specially addressed in the calculations. The theoretical equilibrium lattice constant, determined to be 2.83 Å, underestimates the measured value [29] by about 1% with somewhat better agreement with the experiment in the case where non-local corrections are employed. In our analysis, CoAl fails to develop any magnetic ordered state, in agreement with all previous bulk calculations. Nevertheless, it should be mentioned at this stage that slab calculations performed within the full-potential linear augmented-plane-wave (FLAPW) formalism resulted in a magnetic ordering for the CoAl(100) surface [30]. The photoemission experiments shown here are spin-integrated ones and present the intensity distributions only. The main aspect of this contribution consists in a precise band mapping of CoAl along this direction. Therefore, the paramagnetic bulk potentials that we calculated by the procedure described are adequate for a quantitative interpretation of the measured spectra. For the surface potential, a spin-independent surface barrier of Rundgren–Malmström type [7] has been used in order to describe the electronic structure quantitatively in the surface region. Possible damping effects were included in a phenomenological way by adding a layer-independent imaginary contribution $-iV_{i0}$ to the muffin-tin potentials. For the initial state, V_{0i} has been chosen to be energy dependent, with

$$V_{0i1} = 2\arctan(0.1 + 0.0001(x - 0.5)^4).$$

For the final state, we used a value of $V_{0i2} = -1$ eV for a photon energy of 12 eV varying to $V_{0i2} = -2.6$ eV at 28 eV photon energy in our theoretical investigation. Finally, all of the calculated raw spectra were convoluted with a Gaussian with FWHM = 0.2 eV to account for the experimental resolution of the spectrometer.
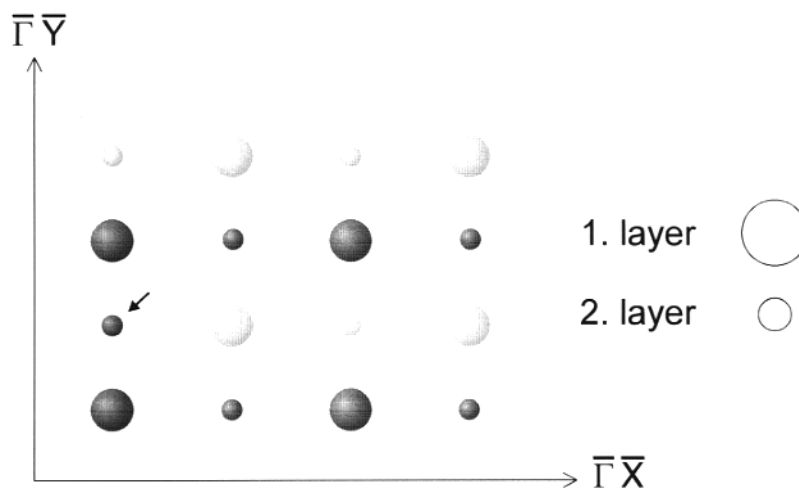

Figure 3. The top view of the (110) surface of CoAl with a Co antistructure atom in the second layer.

4. Structure

The β-phase of CoAl crystallizes in a CsCl structure with a lattice constant of 2.86 Å [29]. For our photoemission analysis we have used the theoretical lattice constant of 2.81 Å, which is about 1% smaller than the measured one. The corresponding relativistic bandstructure along ΓM is shown in figure 1. It has been calculated by using the TB-LMTO potentials in our photoemission code based on a relativistic Korringa–Kohn–Rostoker (KKR) multiple-scattering formalism. Spin–orbit coupling leads to a cancellation of the energy degeneracy of the Σ_5^3 and Σ_5^2 bands at the symmetry points Γ and M. Also, as a consequence of relativistic effects, the crossing of the lower Σ_5^1 and Σ_5^4 bands is now forbidden.

It has been determined by *I–V* LEED measurements that the distance between the Co atoms of the first and second layer is 0.4% larger than the bulk value. The corresponding
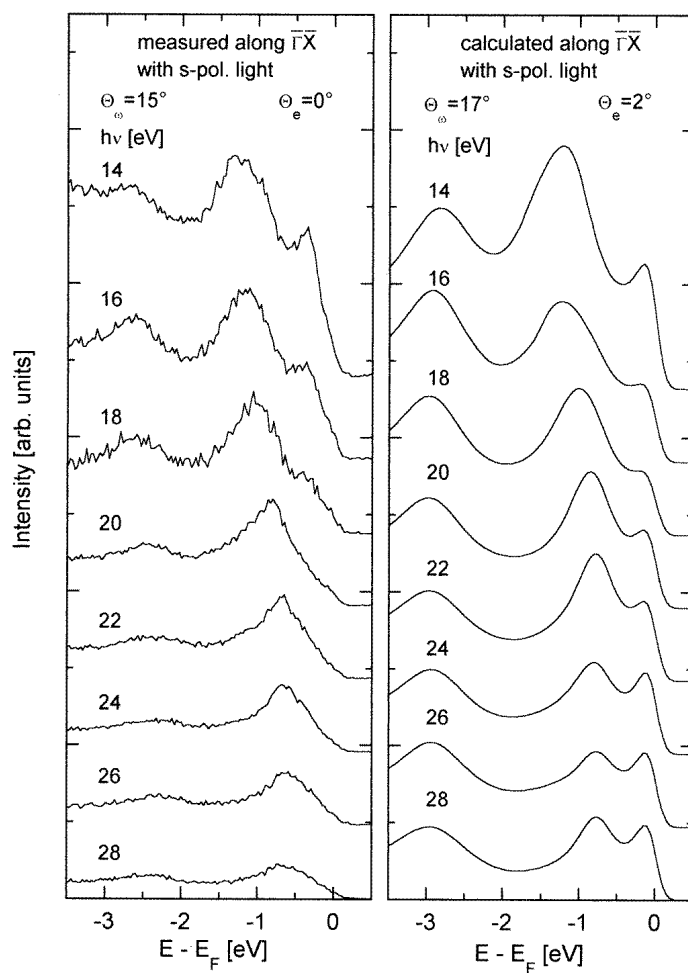

Figure 4. A series of normal-emission spectra for different photon energies obtained using s-polarized light along $\overline{\Gamma}\,\overline{X}$. Left: experimental spectra; right: calculated spectra ($\Theta_\omega = 17°$; $\Theta_e = 2°$).
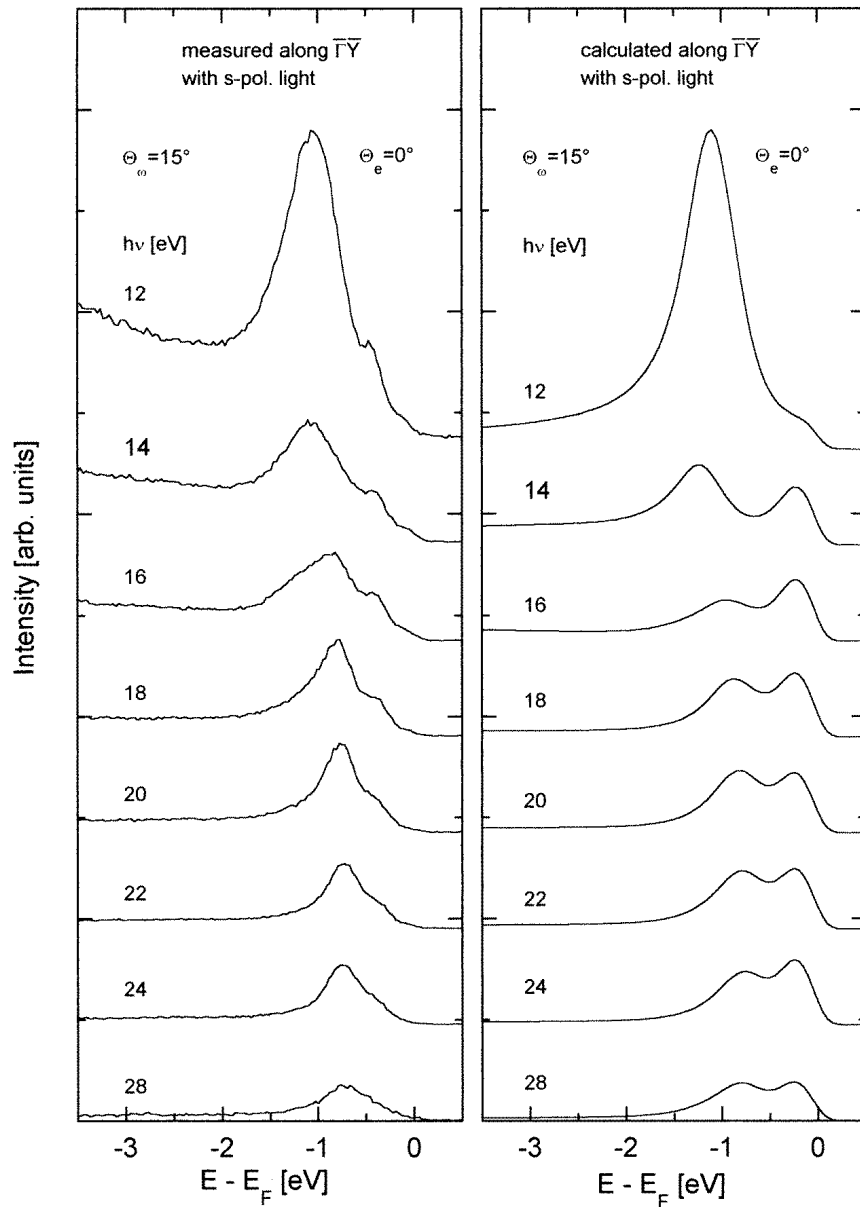
Figure 5. A series of normal-emission spectra for different photon energies obtained using s-polarized light along $\overline{\Gamma}\,\overline{Y}$. Left: experimental spectra; right: calculated spectra ($\Theta_\omega = 15°$; $\Theta_e = 0°$).

value for the Al atoms is 4.7%. To take into account this structural behaviour, we have performed photoemission calculations for a half-infinite crystal with a rumpled layer as the first bulk layer. By considering the net relaxation of about 0.4% together with the rumpling of the Al atoms, it was possible to reduce the intensity ratio of the main peaks from 63% to 39%. The experimental value is 23%. This result is shown in figure 2

as a series of calculated spectra for excitation energies between 14 and 28 eV. Because we were able to reproduce the correct trends in our photoemission calculations, it follows that the intensity ratio is mainly determined by multiple-scattering effects, which we have considered via a rumpled layer. Further improvements in the photoemission analysis can be expected from using layer-dependent potentials resulting from a slab calculation or by applying a Green's-function formalism. It is known that B2 transition metal aluminides inhibit high concentrations of point defects [31]. Combinations of vacancies on transition metal sites and so-called antistructure atoms are predominant. This means that transition metal atoms substitute for Al atoms. LEED studies, for example, indicate a 20% surplus of Co in the second layer [32]. In order to take into account these structural properties in our photoemission investigation on CoAl, we used a four-times-larger unit cell with a Co antistructure atom. Figure 3 shows the additional Co atom (arrow), which is located 0.05 Å above the second-layer Al position. Although our approximation can be seen as a first step only, considerable improvement has been achieved in the calculated spectra as compared with the experimental data. This will be shown later on. A more sophisticated approach to the disorder and to the onset of magnetism in CoAl and other transition metal aluminides consists in the coherent potential approximation (CPA). Photoemission calculations based on this method should unambiguously result in a further improved agreement with our experimental photoelectron spectra. We concentrate in this contribution mainly on the ordered structure of CoAl; in two forthcoming publications the electronic structure of disordered FeAl, CoAl and NiAl and the corresponding photoemission intensities will be discussed in more detail within the CPA method.
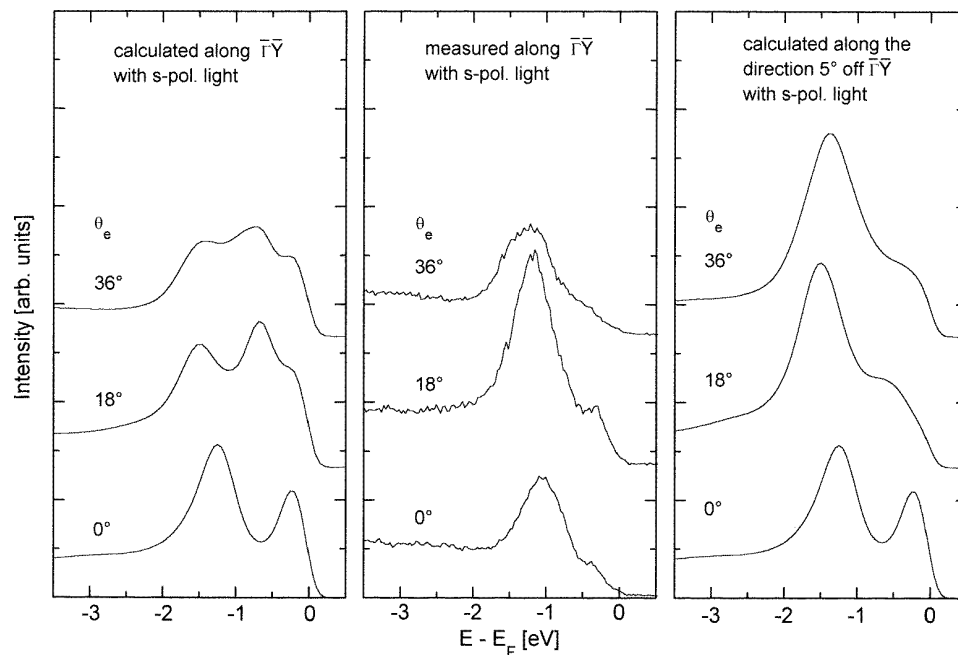

Figure 6. A comparison of measured off-normal-emission spectra (middle) obtained using s-polarized light along $\overline{\Gamma}\,\overline{Y}$ with spectra calculated for different angles between the scattering plane and $\overline{\Gamma}\,\overline{Y}$. Left: $\phi = 0°$; right: $\phi = 5°$.

5. Results for the ordered structure

At first we show a series of normal-emission spectra ($\Theta_e = 0$ for different photon energies obtained using s-polarized light along $\overline{\Gamma}\,\overline{X}$ (figure 4). To achieve a better agreement with the experimental curves, the calculations were performed for an angle of incidence of $\Theta_\omega = 17°$ and an emission angle of $\Theta_e = 2°$. The difference from the experimental set-up lies within the inaccuracy of the measurement. In general we observe a good agreement between experimental and calculated spectra. The peak at about -1 eV arises due to direct $\Sigma_5^1 \to \Sigma_5^1$ transitions. The decrease in intensity and the shift to lower binding energies with increasing photon energy is very well reproduced. The intensities of the other peaks, namely near E_F and at -3 eV, which are due to direct $\Sigma_5^4 \to \Sigma_5^1$ transitions, are overestimated at higher excitation energies. The difference in the positions of the peaks, especially for the Σ_5^4
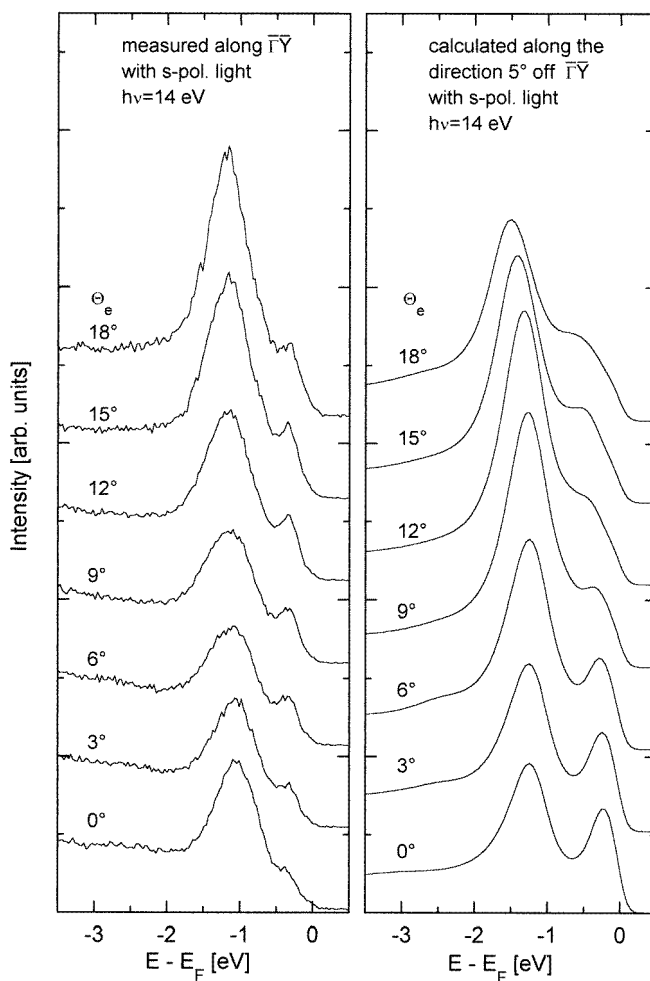

Figure 7. A series of spectra for different angles of emission obtained using s-polarized light ($h\nu = 14$ eV) along $\overline{\Gamma}\,\overline{Y}$. In the calculations the scattering plane is rotated by $5°$ around the surface normal. Left: experimental spectra; right: calculated spectra ($\Theta_\omega = 15°$).

state with the highest binding energy (i.e. -3 eV), are probably due to correlation effects not included in the LDA framework. In figure 2 we show a comparison between experimental and calculated normal-emission spectra for p-polarized light ($\Theta_\omega = 75°$; $\Theta_e = 0°$) along $\overline{\Gamma}\,\overline{X}$. Again the dispersion and the course of the intensity of the Σ_5^1 peak at about -1 eV are quantitatively reproduced. The peak with the highest binding energy is also due to a direct $\Sigma_5^1 \rightarrow \Sigma_5^1$ transition. The intensity ratio is correct but the energy positions of this peak differ by 0.3 to 0.4 eV compared to the experimental values. The peak near the Fermi level which can be seen in the experimental spectra for photon energies of 14 and 16 eV could not be reproduced in the calculations.

The next figure (figure 5) shows a series of normal-emission spectra for s-polarized light along $\overline{\Gamma}\,\overline{Y}$. The agreement in energetic position and intensity of the Σ_5^3 bulk state between measured and calculated curves is again very good. The intensity of the non-dispersing
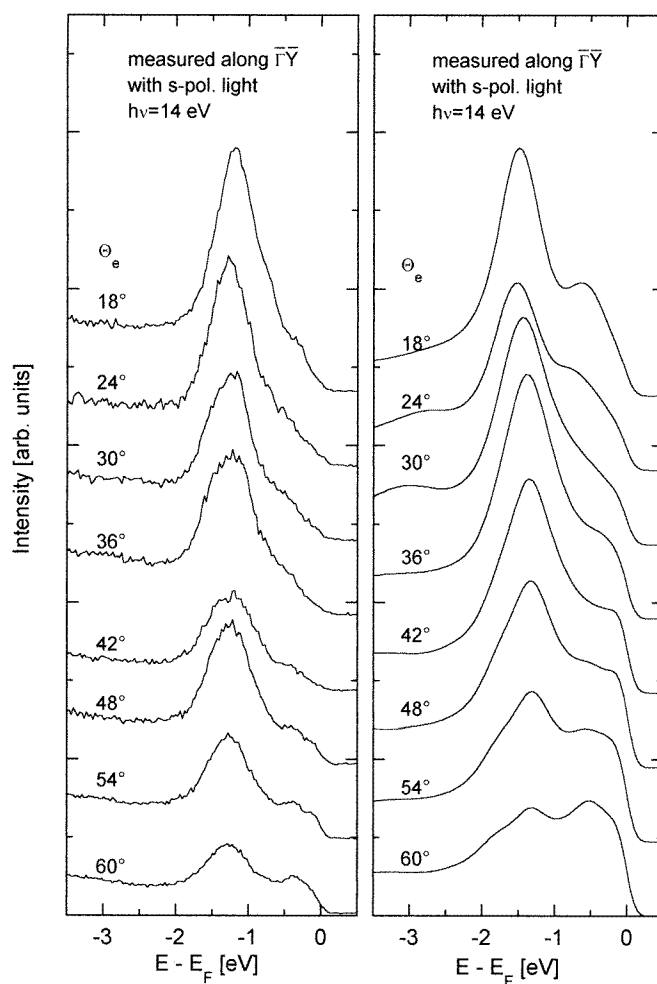

Figure 8. A series of spectra for different angles of emission obtained using s-polarized light ($h\nu = 14$ eV) along $\overline{\Gamma}\,\overline{Y}$. In the calculations the scattering plane is rotated by 5° around the surface normal. Left: experimental spectra; right: calculated spectra ($\Theta_\omega = 0°$).

peak near the Fermi level (-0.4 eV in the experimental spectra, -0.25 eV in the theoretical spectra), which is due to a surface state, seems to be overestimated at higher excitation energies.

For the off-normal-emission spectra we achieve a better agreement with the experiment by rotating the scattering plane about the surface normal. The left-hand panel of figure 6 shows calculated off-normal-emission spectra with the scattering plane parallel to $\overline{\Gamma}\,\overline{Y}$. For higher detection angles an additional peak appears at about -0.75 eV. This peak, which is probably due to a Σ_5^2 state, is not visible in the experimental curves (middle panel) and disappears when the scattering plane is rotated azimuthally by $5°$ (right-hand panel). The series of off-normal spectra shown in figure 7 and figure 8 were calculated with this geometry.

Figure 7 depicts spectra for detection angles from $0°$ to $18°$ and light incidence of $15°$. The Σ_5^3 bulk peak shifts to higher binding energies with increasing emission angles in both experiment and theory. In contrast to the experimental result, the surface state disperses and loses some intensity in the theoretical spectra. This could be an indication of a deviation from the stoichiometric composition at the surface.

For detection angles greater than $18°$ the experiments could be performed with completely s-polarized light (normal incidence). As shown in figure 8 the dispersion of the bulk peak could not be reproduced as accurately for higher emission angles. In the calculated spectra the peak shifts between $18°$ and $60°$ by about 0.2 eV to lower binding
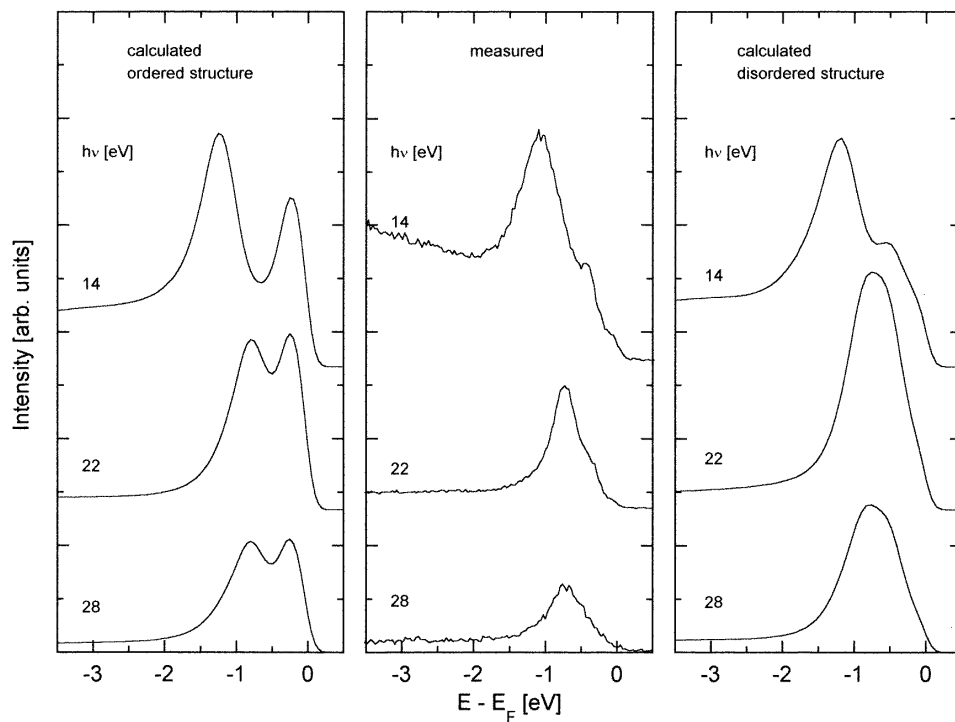

Figure 9. A comparison of measured normal-emission spectra (middle) obtained using s-polarized light along $\overline{\Gamma}\,\overline{Y}$ with spectra calculated for the ordered (left) and disordered structure (right).

energies whereas in the experimental curves it disperses by about 0.1 eV in the opposite direction. At detection angles of 54° and 60° a shoulder at -1.8 eV is visible in the theoretical spectra, which might be due to excitation of a Σ_5^2 state. This feature is not resolved in the experimental curves.

6. Results for the disordered structure

In figure 9 we compare calculated spectra for the ordered and disordered structure with the corresponding experimental data. It is clearly visible that the agreement between experiment and theory is improved by taking into account an antistructure atom. For all three different excitation energies, the peak positions as well as the intensity ratios are found to be closer to the experiment. In particular, the surface state located near the Fermi edge is shifted slightly to higher binding energies. An explanation can be found in the change of the electronic structure induced by the supercell geometry, which should influence the energetic position and intensity of a bulk-like surface state. As one would expect, another effect of the simulated disordering consists in a broadening of the intensity distributions. This is also shown in figure 10, which depicts a series of normal-emission spectra calculated for p-polarized light. Even when the overall agreement between experiment and theory is very good, some details could be improved. For example, the calculated intensity ratios should
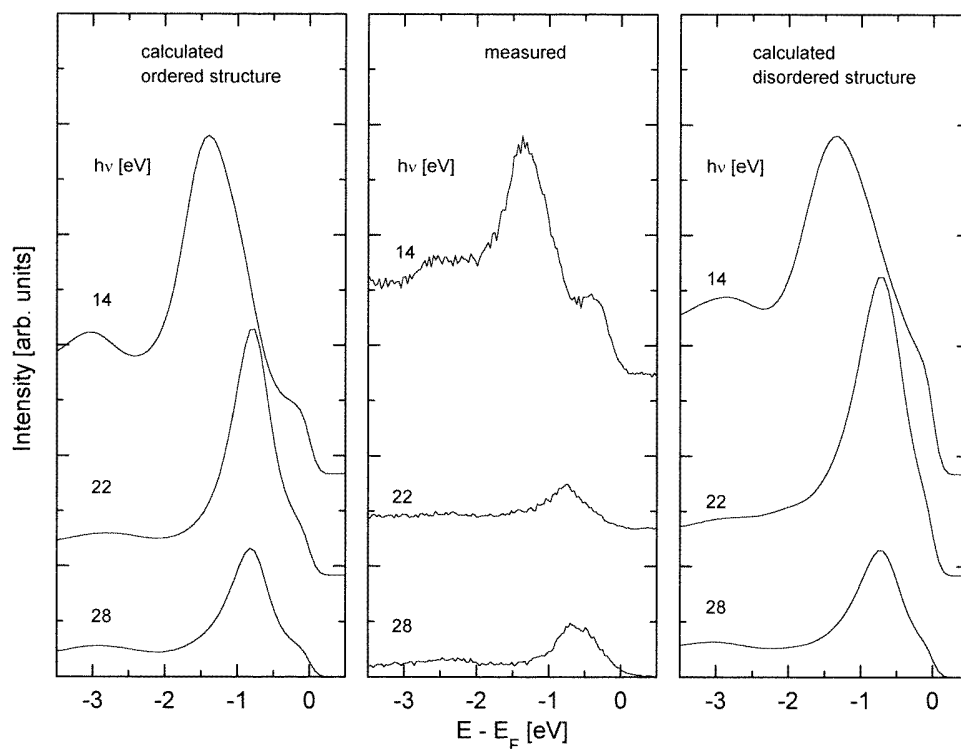

Figure 10. A comparison of measured normal-emission spectra (middle) obtained using p-polarized light along $\overline{\Gamma}\,\overline{X}$ with spectra calculated for the ordered (left) and disordered structure (right).

decrease for increasing photon energies for both cases. A CPA photoemission investigation based on the correct configurational average is expected to produce these experimental findings.

7. Summary

We have presented calculations of photoemission spectra of CoAl(110) and compared these results with experimental data [10].

For the ordered structure the overall agreement between theoretical and experimental curves is very satisfactory. The position and dispersion of the bulk and surface states appearing could be reproduced very well over a wide range of excitation energies and for different polarizations. The deviations for the more tightly bound states could be due to correlation effects. Further improvement, especially for the intensity ratio, should also be achieved by using the full-potential photoemission theory in which the transition-matrix elements are calculated for atomic potentials with non-spherical contributions.

Since CoAl persists over a wide range of composition, we have tried to simulate a partially disordered structure by using a larger unit cell with a Co antistructure atom in the second layer. This leads to an improvement in the position of the bulk-induced surface state and to a broadening of the bulk peaks. At the same time the calculations for s-polarized light along $\overline{\Gamma}\,\overline{X}$ show less agreement with experimental spectra. An improvement might be achieved by using larger unit cells and considering vacancies in the Co sublattice. Performing CPA photoemission calculations should lead to a better agreement between experiment and theory.

References

[1] Pendry J B 1976 *Surf. Sci.* **57** 679
[2] Thörner G and Borstel G 1984 *Phys. Status Solidi* b **126** 617
[3] Ackermann B and Feder R 1985 *J. Phys. C: Solid State Phys.* **18** 1093
[4] Braun J, Thörner G and Borstel G 1985 *Phys. Status Solidi* b **130** 643
[5] Ginatempo B, Durham P J and Gyorffy B I 1989 *J. Phys.: Condens. Matter* **1** 6483
[6] Braun J and Borstel G 1993 *Phys. Rev.* B **48** 14 373
[7] Malmström G and Rundgren J 1980 *Comput. Phys. Commun.* **19** 263
[8] Getzlaff M, Bansmann J, Braun J and Schönhense G 1997 *J. Magn. Magn. Mater.* **161** 70
[9] Ufer H 1996 private communication
[10] Castro G R 1996 private communication
[11] Müller Ch, Blau W and Ziesche P 1983 *Phys. Status Solidi* b **116** 651
[12] Fleischer R L, Dimidick D M and Lipsitt H A 1989 *Annu. Rev. Mater. Sci.* **19** 231
[13] Butler R, Hanlon J E and Wasilewski R J 1969 *J. Phys. Chem. Solids* **30** 1929
[14] Stefanou N, Zeller R and Dederichs P H 1987 *Phys. Rev.* B **35** 2705 and references therein
[15] Davis H L and Noonan J R 1985 *Phys. Rev. Lett.* **54** 566
[16] Chen S P, Voter A F and Srolovitz D J 1986 *Phys. Rev. Lett.* **57** 1308
[17] König U, Redinger J, Weinberger P and Stocks G M 1987 *Phys. Rev.* B **35** 8243
[18] Lui S-C, Kang H, Mele E J, Plummer E W and Zehner D M 1989 *Phys. Rev.* B **39** 13 149
[19] Lui S-C, Davenport J W, Plummer E W, Zehner D M and Fernando G W 1990 *Phys. Rev.* B **42** 1582
[20] Braun J 1996 *Rep. Prog. Phys.* **59** 1267
[21] Andersen O K 1975 *Phys. Rev.* B **19** 3060
[22] Andersen O K and Jepsen O 1984 *Phys. Rev. Lett.* **53** 2571
[23] Moruzzi V L and Marcus P M 1993 *Phys. Rev.* B **47** 7878
[24] von Barth U and Hedin L 1972 *J. Phys. C: Solid State Phys.* **5** 1629
[25] Lambrecht W R R and Andersen O K 1983 *Phys. Rev.* B **34** 2439
[26] Kobayashi S and Fujiwara T 1997 *Phys. Rev.* B **55** 7445
[27] Langreth D C and Mehl M J 1981 *Phys. Rev. Lett.* **47** 446

[28] Langreth D C and Mehl M J 1983 *Phys. Rev.* B **28** 1809
[29] Hansen M and Anderko K 1958 *Constitution of Binary Alloys* (New York: McGraw-Hill)
[30] Ostroukhov A A, Floka V M and Cherepin V T 1996 *Surf. Sci.* **352–354** 919
[31] Wasilewski R J 1968 *J. Phys. Chem. Solids* **29** 39
[32] Blum V, Rath C, Castro G R, Kottke M, Hammer L and Heinz K 1996 *Surf. Rev. Lett.* **3** 1409